Optical and Quantum Electronics (2024) 56:571
https://doi.org/10.1007/s11082-023-06228-z

Passively Q-switched erbium-doped fiber laser based on two-dimensional boron carbide nanoparticles as saturable absorber

Iman N. Jasem[1] · Hiba H. Abdullah[1] · Mohammed J. Abdulrazzaq[1]

Received: 7 July 2023 / Accepted: 27 December 2023 / Published online: 30 January 2024

Abstract
The utilization of boron carbide nanoparticles (B_4C) as a saturable absorber (SA) for generating pulses by a fiber laser operating in Q-switched mode is the subject of our investigation, the findings of which are presented. This was accomplished by combining boron carbide nanoparticles (B_4C-NPs) with polyvinyl alcohol (PVA) to form a thin-film-based SA. This SA was then placed within an erbium-doped fiber laser (EDFL) in a ring cavity configuration to enable passive Q-switching operation. The modulation depth of the B_4C-SA was 2.3%. Stable Q-switching laser operation was accomplished with a pump power of 180 mW and central wavelength of 1561 nm by producing laser pulses with a pulse duration of 15.27 µs and pulse repetition rate of 31.6 kHz. A comparable pulse energy, which was attained at the maximum pump power of 275 mW, was approximately 2.61 nJ. The radio-frequency spectrum was examined to verify the pulse stability. The study showed a signal-to-noise ratio of 35 dB. These results expand the potential of B_4C-based saturable absorbers, making them strong contenders for innovative photonic devices.

Keywords Passively Q-switched fiber laser · Ring cavity · Saturable absorber · 2D material · Boron carbide (B_4C)

1 Introduction

Pulsed lasers have been extensively utilized in various fields (Kim et al. 2023). In contrast, to continuous-wave lasers, they offer greater versatility in adjusting parameters such as peak power, pulse duration, and pulse repetition rate (Jiang et al. 2020). Q-switching has been the primary method of generating stable pulse trains whose pulse duration is in the

✉ Mohammed J. Abdulrazzaq
mohammed.j.abdulrazzaq@uotechnology.edu.iq

Iman N. Jasem
iman.n.jasem@uotechnology.edu.iq

Hiba H. Abdullah
hiba.h.abdullah@uotechnology.edu.iq

[1] Laser and Optoelectronics Engineering Department, University of Technology-Iraq, Baghdad, Iraq

range of microseconds (Jasem et al. 2023). Microsecond-pulsed lasers have unusual uses, including laser ablation for material processing and surgical treatments, because they can store large amounts of energy in relatively long pulse lengths (Du et al. 2007; Siniaeva et al. 2009; Tu et al. 2014; Seifert et al. 2021).

McClung et al. developed the first Q-switched pulse laser in 1960 (McClung and Hellwarth 1962). Since then, the high pulse energy and short pulse duration of Q-switched fiber lasers have proved to be desirable characteristics. There are many applications for the Q-switched fiber laser, including optical communication (Liu et al. 2020a), biomedicine (Wang et al. 2019), military, and materials micromachining (Liu et al. 2020b). Depending on the components that are used as Q-switches, they may be referred to as active Q-switched lasers and passive Q-switched lasers (Shakaty et al. 2022). A typical method for producing passively Q-switched lasers is to use a thin film as a saturable absorber (SA) to convert a continuous wave (CW) output into a periodic pulse train (Hassan et al. 2020). Various SAs have been developed for passive Q-switched operation (Mao et al. 2017a). These SAs incorporate materials with polymers (Hassan et al. 2019), micro-fibers (Luo et al. 2013), side-polished fibers (Mao et al. 2016), or fiber facets (Sobon et al. 2012). Despite their high cost and rather narrow operating wavelength ranges, the first successful use of semiconductor SA mirrors has started a new trend in passive Q-switching (Fluck et al. 1997; Muhammad et al. 2022). However, researchers are driven to further explore different materials as the new generation for SA because of limited bandwidth and a complex construction process (Ismail et al. 2020). It began with three-dimensional (3D) materials like iron-doped crystal (Bret and Gires 1964). Followed by Graphene which is a 2D material with the best SA for Q-switching and mode-locking operation due to its low modulation depth and broadband saturable absorption (Hassan et al. 2019). Two-dimensional nanomaterials have become a popular choice for SAs in pulsed fiber lasers (Zhang et al. 2010) due to their exceptional nonlinear absorption properties, particularly their saturable absorption properties (Guo et al. 2015).

Other 2D materials are transition metal dichalcogenides such as (Molybdenum disulfide (MoS_2) and Tungsten disulfide (WS_2) (Chen et al. 2015; Wu et al. 2015)), topological insulators (TI) (Luo et al. 2013), Boron Nitride (BN) (Liu et al. 2021), as well as one-dimensional (1D) nanomaterials (Wu et al. 2016), have attracted significant research interest. These materials, known for their geometric symmetry, carrier confinement, and adjustable bandgap, provide an excellent foundation for nanoscale saturable absorber (SA) studies (Yadav et al. 2017). These nanomaterials, typically derived from semiconducting or metallic sources, offer a unique platform for advancing SA research at the nanometer level (Xia et al. 2003). Furthermore, zero-dimensional quantum dots (QDs) nanomaterials such as cadmium selenide (Bret and Gires 1964), and lead sulfide/Cadmium sulfide (PbS/CdS) (Yang et al. 2022) have been proven to exhibit saturable absorption characteristics.

The focus of optoelectronics research has shifted to finding semiconductive materials with intriguing optical characteristics. Ceramics are a unique class of materials with intriguing physical, chemical, electrical, and optical characteristics that make them ideal for use in fiber optics, sensors, medical implants, the automotive industry, and other fields (Saritha Devi et al. 2018). Boron carbides (B_4Cs) are ceramic compounds that are distinguished by a distinctive blend of features, rendering them the preferred material for a wide range of engineering purposes due to their excellent mechanical, refractory, and semi-conducting qualities (Pierson 1996). Boron carbide finds utility in refractory settings because of its exceptional resistance to high temperatures and thermal stability. It serves

as an abrasive powders and coating owing to its remarkable durability against abrasion. Its superior hardness and low density make it outstanding for ballistic applications, and it is frequently utilized in nuclear contexts for absorbing neutron radiation. Furthermore, boron carbide operates as a high-temperature semiconductor, holding promise for innovative electronic uses (Mondal and Banthia 2005). It is a promising material in Q-Switching and modelocked laser technology with a wide range of uses due to its excellent nonlinear properties. Two-dimensional B_4C nanostructures are a promising platform for creating hybrid structures (Tao et al. 2010), enhancing the structural and mechanical characteristics of metal matrix composites (Alizadeh et al. 2013), serving as substitutes for traditional semiconductors and delivering high energy density (Bao 2010), among the many types of nanostructures available (Nersisyan et al. 2015). B_4C is sometimes referred to as a 'black diamond' due to its higher level of hardness – it is the third hardest substance after diamond and cubic boron nitride (Caretti et al. 2008). The p-type semiconducting B_4C has three linearly organized CBC or CBB chains and twelve icosahedrons that are covalently bound to one another. B_4C has good electrical, optical, and luminescent characteristics, making it a potential light emitter (Thevenot 1990). Therefore, there is a great deal of potential in 2D B_4C processing and applications (Guo et al. 2021).

This paper introduces and highlights the utilization of boron carbide (B_4C)-NPs-based SAs in passively Q-switched erbium-doped fiber lasers (EDFLs). To leverage the saturable absorption properties of B_4C-NPs, a film of B_4C and polyvinyl alcohol (PVA) was prepared by embedding the nanoparticles into a PVA host. The film was integrated into an EDFL fiber cavity, resulting in the generation of Q-switched pulse trains with a minimum pulse duration of approximately 15.27 µs. The pulse repetition rate and pulse energy were measured at 31.6 kHz and 2.61 nJ, respectively.

2 Fabrication and characterization of boron carbide-SA

In this experiment, the solution casting method was used to prepare the B_4C/polymer composite to fabricate SAs. This method is preferable for preparing the SA films of nanoparticles because it is a simple, easy, and rapid method compared to other methods. The utilization of PVA solution as a host polymer is crucial due to its excellent film-forming properties (Baharom et al. 2019), exceptional flexibility (Norizan et al. 2018), water solubility, transparency, non-toxicity, and high durability (Sadeq et al. 2018). In addition, the sodium dodecyl sulphate (SDS) solution contributes to the process of homogenizing the prepared thin film.

The B_4C/PVA SA can be fabricated using the following steps. To begin with, a solution was prepared by dissolving 1 g of SDS in 100 ml of deionized water using a magnetic stirrer for 30 min at room temperature. Concurrently, a PVA solution was created by combining 1 g of PVA with 100 ml of deionized water and stirring at 60°C for approximately one hour. Next, 2 ml of deionized SDS solution was blended with 15 mg of B_4C powder using a magnetic stirrer for two hours. Then, 3 ml of PVA solution was mixed into the B_4C/SDS solution and stirred for an hour. After being mixed, the solution underwent ultrasonication for approximately 45 min to avoid aggregation. Eventually, the resulting mixture was carefully transferred into a glass petri dish and left to air-dry at room temperature for 4 days until a film made of B_4C/PVA was formed.

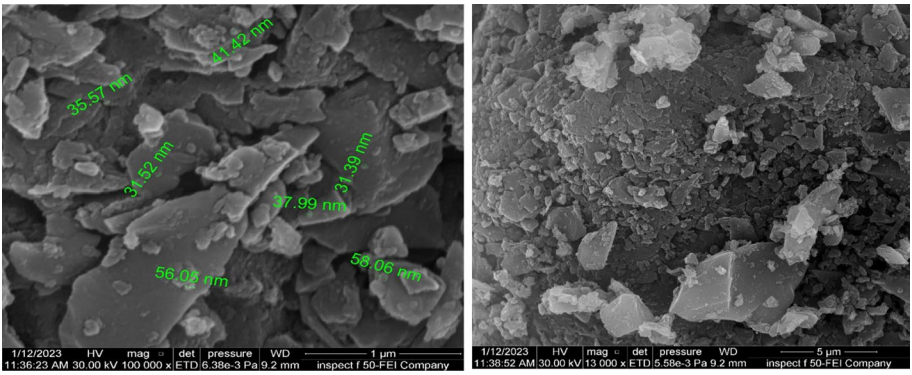

Fig. 1 SEM images with different magnifications of the using B_4C powder

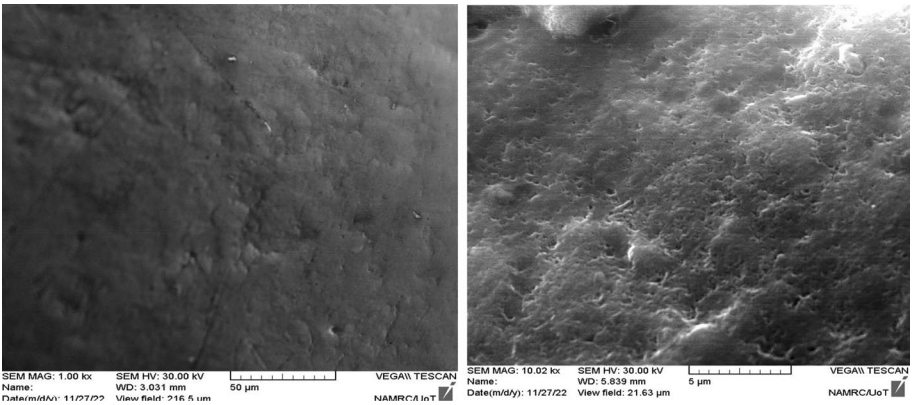

Fig. 2 Scanning electron microscopy image of B_4C/PVA thin film

Various methods were employed to determine the composition, size, and purity of the nanoparticles that were used. The morphology of the B_4C powder was examined using scanning electron microscopy (SEM) to observe the particle shape. The SEM image of the B_4C powder can be seen in Fig. 1 at various magnifications. The image shows that the powder particles are evenly distributed and mostly blocky in shape, with a few rectangular particles scattered throughout. Figure 2 shows the SEM image of a thin film made of B_4C/PVA, where multiple particles have combined to create a uniform and consistent surface.

To confirm the elemental composition of the nanoparticles, energy-dispersive X-ray spectroscopy was performed, and the results are presented in Fig. 3. The analysis revealed that the composition of the nanoparticles is primarily carbon and boron, with a small amount of oxygen, iron, and silicon. The presence of oxygen may be due to the formation of B_2O_3 on the B_4C particles, as B_4C is known to absorb oxygen easily and form B_2O_3 on its surface. The atomic percentage of B/C in the B_4C in this study was 2.8, while the expected atomic percentage based on molecular weight should be 2.9, indicating the presence of some free carbon. The presence of free carbon suggests that some boron has

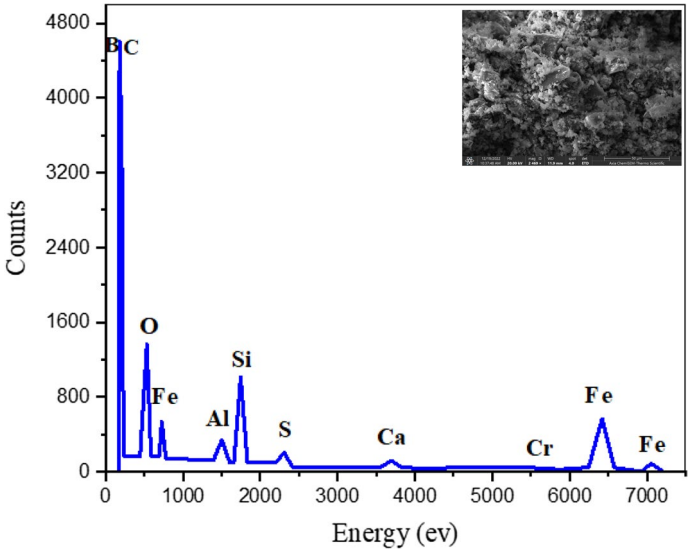

Fig. 3 The energy-dispersive x-ray analysis of the using B_4C nanoparticles

been lost during the reaction, and the amount of free carbon measured was approximately 1.1%. Figure 4 presents the chemical compositions of B_4C-NPs, which have been validated through energy-dispersive spectrum elemental mapping images of B, C, O, Fe, and Si.

The crystalline structures of B_4C-NPs and B_4C/PVA thin film were measured using X-ray diffraction (XRD) as shown in Fig. 5. Figure 5a uses a continuous scan model with generator settings at 30 mA and 40 kV in the range of 5°–65°. The peaks with 2-θ values are 19.7919°, 22.7532°, 23.5236°, 31.9077°, 34.7420°, and 37.4358°, corresponding to JCPDS card No. (96-412-4698). The sharp peaks show that the material has an excellent crystalline structure, thus proving the presence of B_4C and agreeing with the XRD results (Chang et al. 2007). The XRD pattern of B_4C/PVA film has shown in Fig. 5b using a continuous scan model at a wavelength of 1.54060 Å and generator settings at 30 mA and 40 kV in the range of 10–90°. It appears in this form as a result of the presence of PVA with B_4C-NPs in the precipitation of B_4C/PVA films.

Other important parameters to evaluate are the linear and nonlinear absorption characteristics. The linear absorption profile can be observed by illuminating the B_4C film with a white light source. Figure 6a illustrates the absorptive region of the B_4C film spanning from 1525 to 1570 nm. As depicted in this figure, the linear absorption at a wavelength of 1561 nm is measured to 41%. Therefore, the B_4C should be one kind of semiconductor with wide bandgaps. Absorption edges varied with carbon content. Figure 6b shows the UV–visible absorption spectrum for B_4C/PVA nanocomposites. To investigate the band structures of the semiconducting nanoparticles, the bandgap of B_4C was determined using Tauc's method with the assistance of a UV–visible spectrophotometer (Haryński et al. 2022). The calculation process is outlined below:

$$\alpha h\nu = \mathrm{C}(h\nu - \mathrm{Eg})^{\mathrm{n}} \tag{1}$$

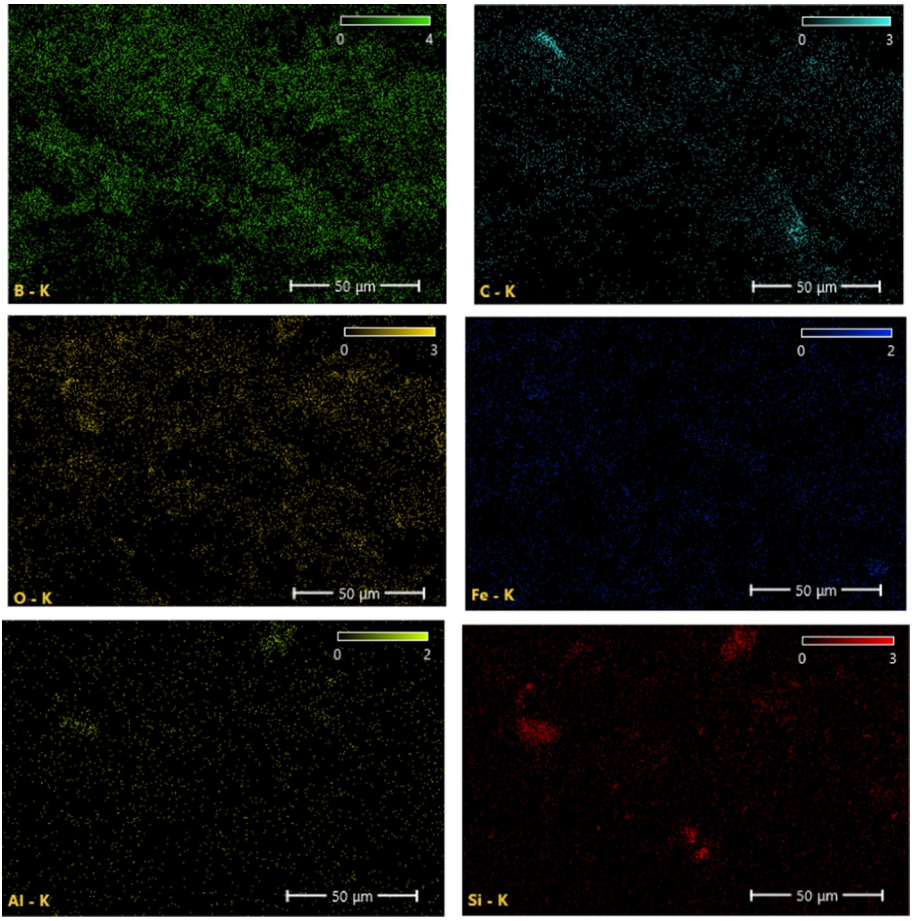

Fig. 4 Energy Dispersive Spectroscopy (EDS) analysis of B_4C-NPs

where Eg is the bandgap energy, h is Planck's constant, ν is the photon's frequency, C is a constant, α is the absorption coefficient, and n is 2 for an indirect band gap. The bandgap energy Eg of the sample can be obtained by extrapolating the linear portion of Tauc's plot to $(\alpha h\nu)^2 = 0$. The bandgap energy determined from Tauc's method is plotted in Fig. 6b and is equal to 3.5 eV.

The nonlinear optical properties of B_4C/PVA thin film were characterized using the Z-scan technique. A schematic of the experimental setup is depicted in Fig. 7. A continuous-wave diode-pumped solid-state laser Nd: YAG (DPSSL) (ALPHALAS) with a wavelength of 1064 nm, power of 100 mW, and a beam diameter of 2 mm was used. A 10 cm focal length lens was used to focus the laser beam into the sample. The thin film sample was placed on a glass slide mounted on a movable holder to vary its position along the Z-axis. This allowed the relationship between the variation in Z value and light intensity to be measured by using a 1 mm diameter pinhole aperture and a photodetector. To determine the nonlinear refractive index (n2) and the nonlinear absorption coefficient (β), both the closed aperture and open aperture methods were employed.

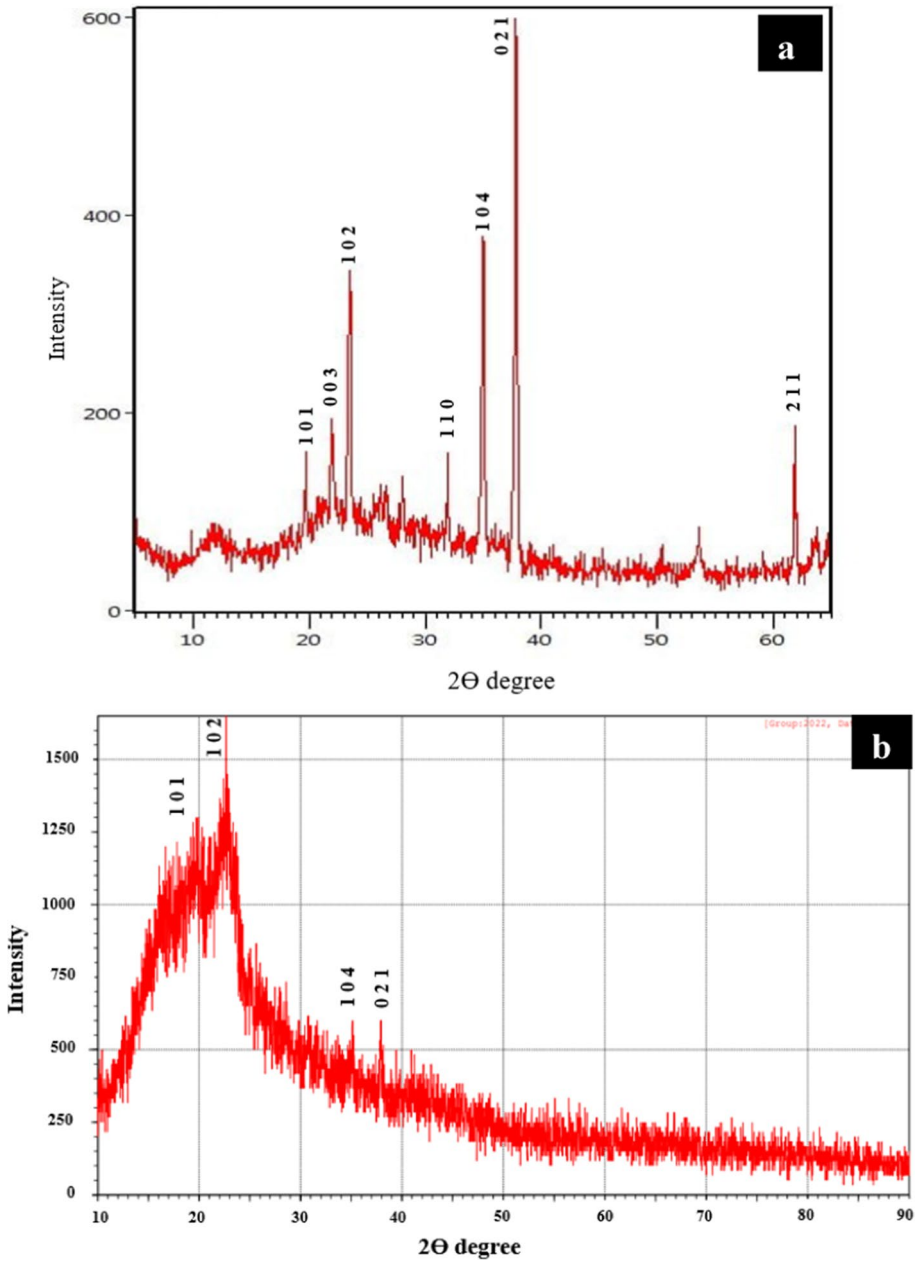

Fig. 5 shows the x-ray diffraction spectrum of **a** B_4C nanoparticles; **b** B_4C/PVA thin film

The modulation depth of the SA was measured by the following equation (Jeon et al. 2015):

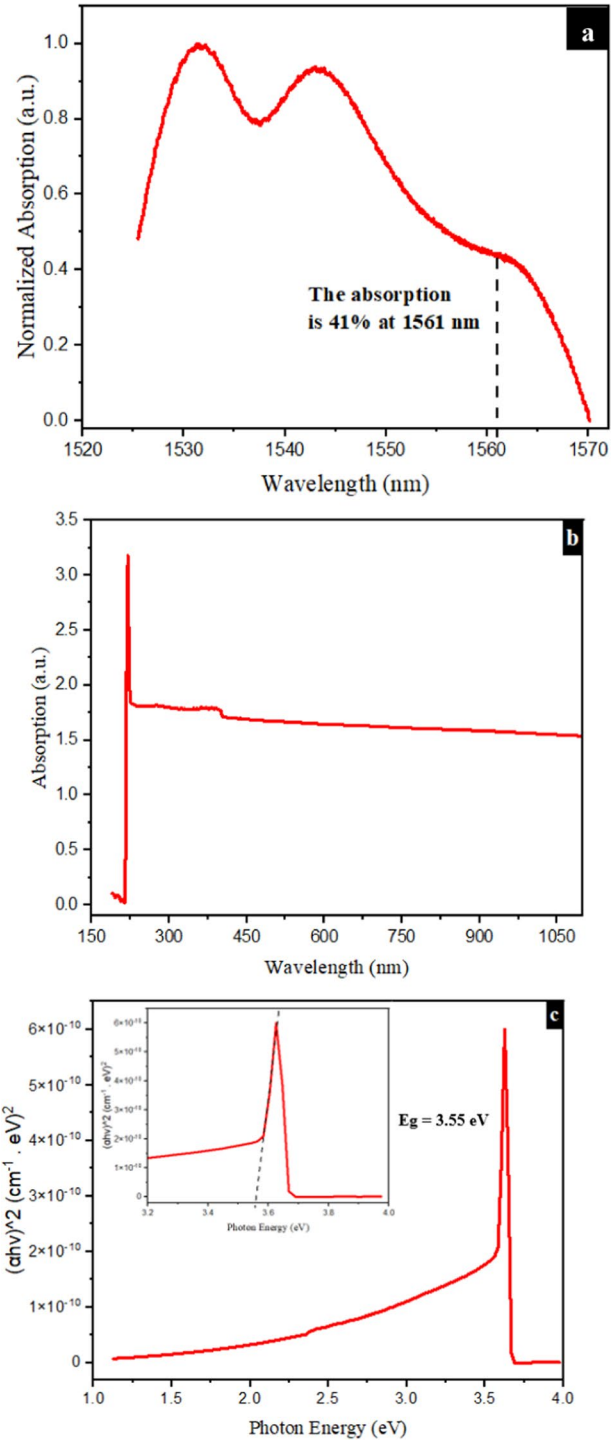

Fig. 6 **a** Linear absorption spectra of the B_4C/PVA, **b** UV–visible spectrum, **c** Tauc's plot, with an inset figure for more explanation of the value of the energy gap

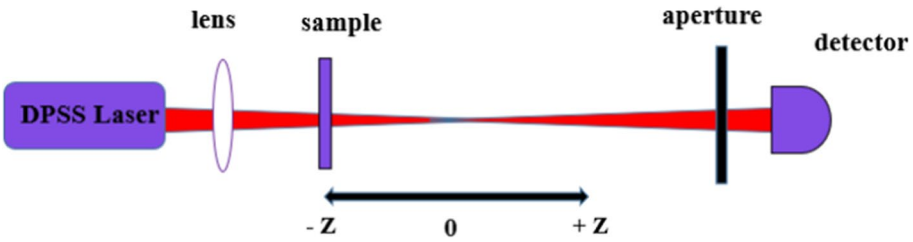

Fig. 7 Z-scan experimental setup

$$\alpha(I) = \frac{\alpha_{\circ}}{1 + \frac{I}{I_s}} + \alpha_{ns} \tag{2}$$

where α_o is the modulation depth, α_{ns} is the non-saturable absorption, I is the light intensity, and I_s is the saturated intensity.

Figure 8 illustrates the Z-scan profiles for both the closed aperture and open aperture measurements. The nonlinear properties are determined by fitting these normalized curves and employing the following equations:

$$n2 = \frac{\Delta\emptyset^{\circ}}{KI^{\circ}L_{eff}} \tag{3}$$

where $\Delta\varnothing_0$ is the phase shift, K is the wavenumber ($2\pi/\lambda$), I_0 refers to the intensity of the laser beam at the focusing point and L_{eff} is the effective length of propagation light inside the sample which is equal to $L_{eff}=(1-e^{(-L\alpha)})/\boldsymbol{\alpha}$ (Abdalhadi et al. 2021).

$$\beta = \frac{2\sqrt{2}\Delta T}{I^{\circ}L_{eff}} \tag{4}$$

where ΔT is the variance between the maximum and minimum transmission (Kumar et al. 2019).

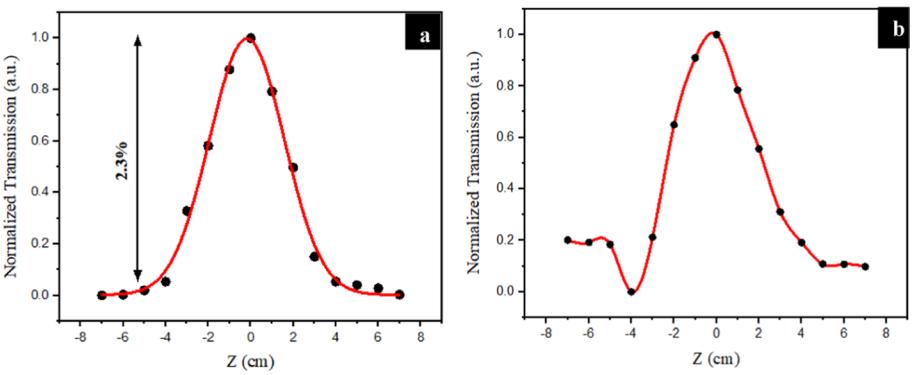

Fig. 8 Z-scan profile for **a** open aperture; **b** closed aperture

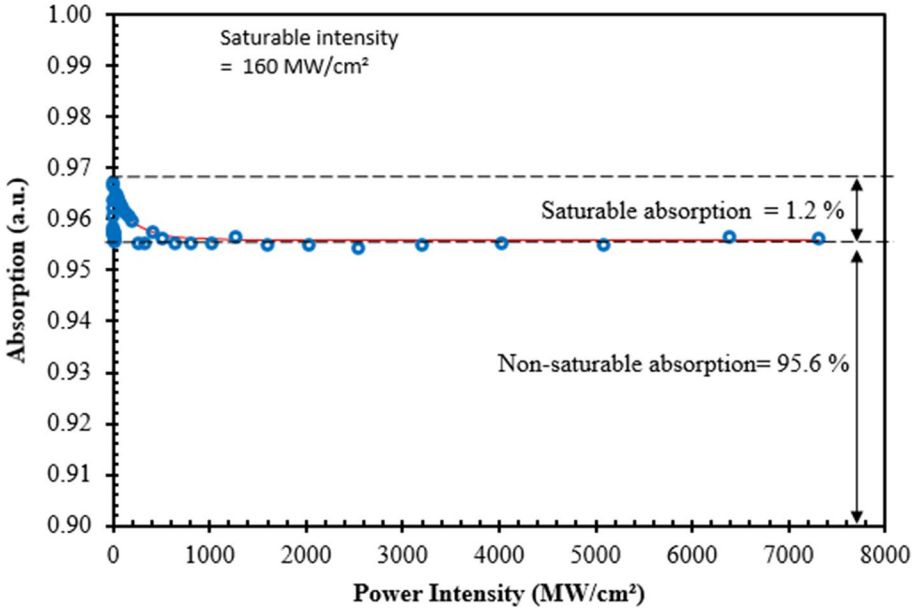

Fig. 9 The nonlinear absorption of the B_4C-SA film

According to the measurement results, the B_4C thin film exhibits a large nonlinear refractive index, absorption coefficient, and modulation depth of 5.591×10^{-6} cm^2/W, 0.011 cm/W, and 2.3%, respectively.

In addition to the z-scan technique, the twin detector balance technique with an ultrashort pulse fiber laser with a pulse duration of 400 fs and repetition rate of 12 MHz at a wavelength of 1550 nm was used, and the nonlinear absorption characteristics were examined. Figure 9 shows the observed absorption data for the B_4C/PVA-SA thin film at various input intensities. The data were fitted using a straightforward two-level saturable absorption model, as shown in Eq. 2. A saturable absorption of 1.2% was observed in the B_4C/PVA thin film, which was defined as the difference between the maximum absorption and nonsaturable absorption loss. The measured saturation intensity is 160 MW/cm^{-2} while the non-saturable absorption is about 95.6%.

3 Experimental setup

The passively Q-switched EDFL configuration is depicted in Fig. 10. The cavity included a 980/1550 nm wavelength division multiplexer (WDM) (THORLABS), a gain medium of 1 m EDF (THORLABS, Liekki ER80-8/125) having a numerical aperture range of 0.13, mode field diameter of 9.5 µm at 1550 nm, and a peak core absorption of 80 dB/m at 1530 nm. An isolator (ISO) (THORLABS) to guarantee the unidirectional propagation of the laser and a 90/10 output coupler (O.C.) were placed in the cavity, where 90% of the light is fed back into the cavity, and the remaining 10% is the laser output. The SA that was manufactured earlier was placed between two fiber ferrules with an FC/UPC connector using an index-matching gel. The EDF is pumped by a 976 nm laser diode (BL976-SAG300) by Temperature Controller with Mount (THORLABS-CLD1015). The optical spectrum

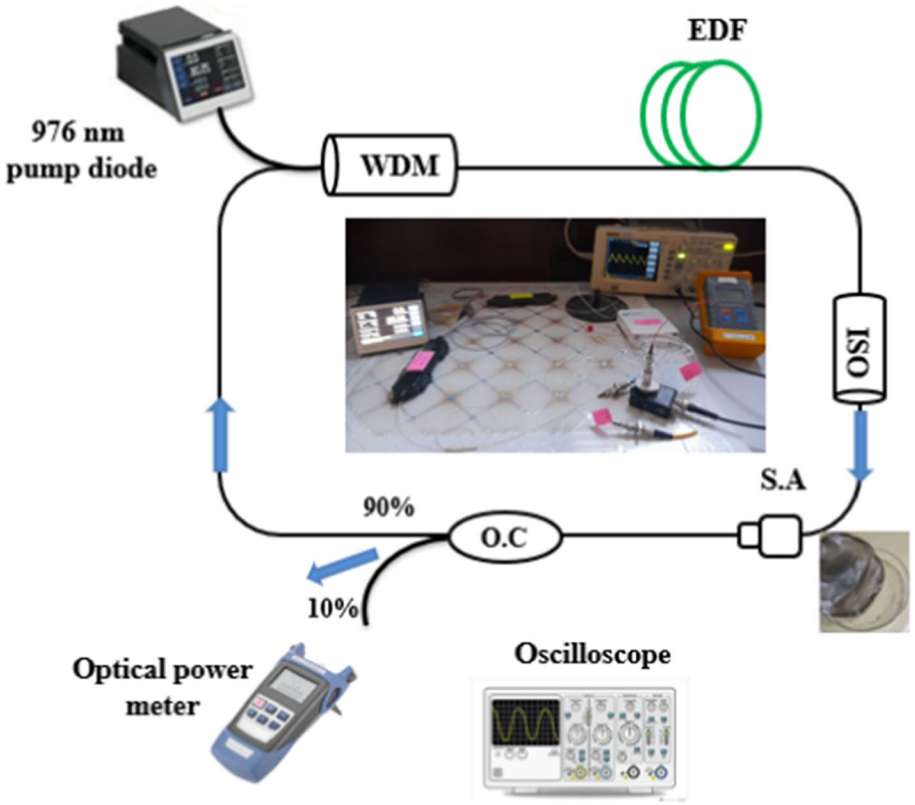

Fig. 10 Laser setup

analyzer (OSA) (Fiber Mini optical spectrum analyzer, 1525–1572 nm is utilized to examine the EDFL spectra with and without the SA, while the output pulse is analyzed with a 2 GHz/s digital storage oscilloscope (OSC) (UNI-T: UTD4102C) through a photodetector is (Thorlabs) DET10C, 700–1800 nm. Additionally, an optical power meter is used to measure the output power. The full length of the cavity is about 3 m.

4 Results and discussion

Continuous wave lasing of the system was observed without the presence of B_4C SA in the laser cavity. No pulses were generated based on this setting. However, when the B_4C SA was introduced into the laser cavity, a steady Q-switched operation was achieved with a threshold power of 180 mW, up to a maximum pump power of 275 mW. Beyond this pump power level, no Q-switched pulses were generated, most likely due to the saturation of the SA, resulting in minimal signal absorption at higher pump powers (Ahmad et al. 2021). The variation of repetition rate, pulse duration, pulse energy, and output power with respect to pump power is presented in Fig. 11. Figure 11a displays the changes in repetition rate and pulse duration at different pumping powers. The repetition rate increases from 9.60 to 31.6 kHz, while the pulse duration exponentially decreases from 40.26 to 15.27

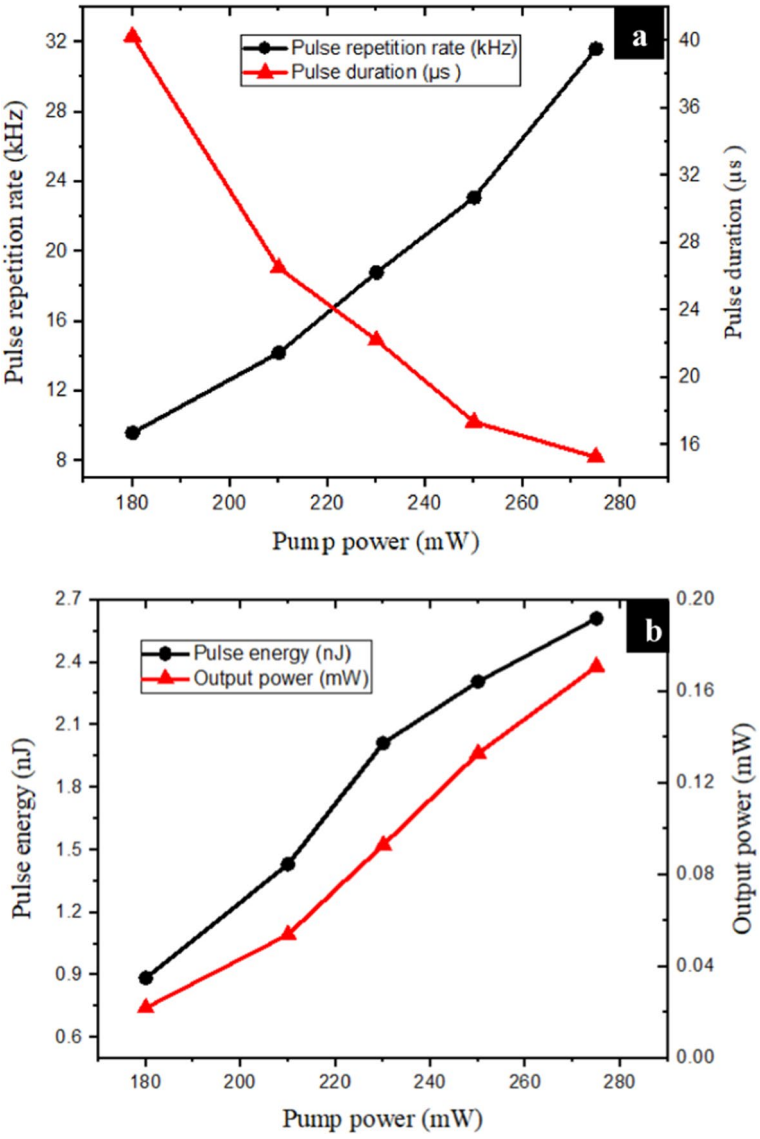

Fig. 11 The characteristics of Q-switched pulses versus pump power

μs as the pump power is raised from the threshold to the maximum value. Additionally, Fig. 11b shows the pulse energy and output power at different pump powers. Both parameters exhibit a linear increase with pump power, with pulse energy rising from 0.885 to 2.61 nJ and average output power increasing from 22 μW to 171 μW. These power-dependent characteristics align well with previous research findings (Al-Hiti et al. 2023).

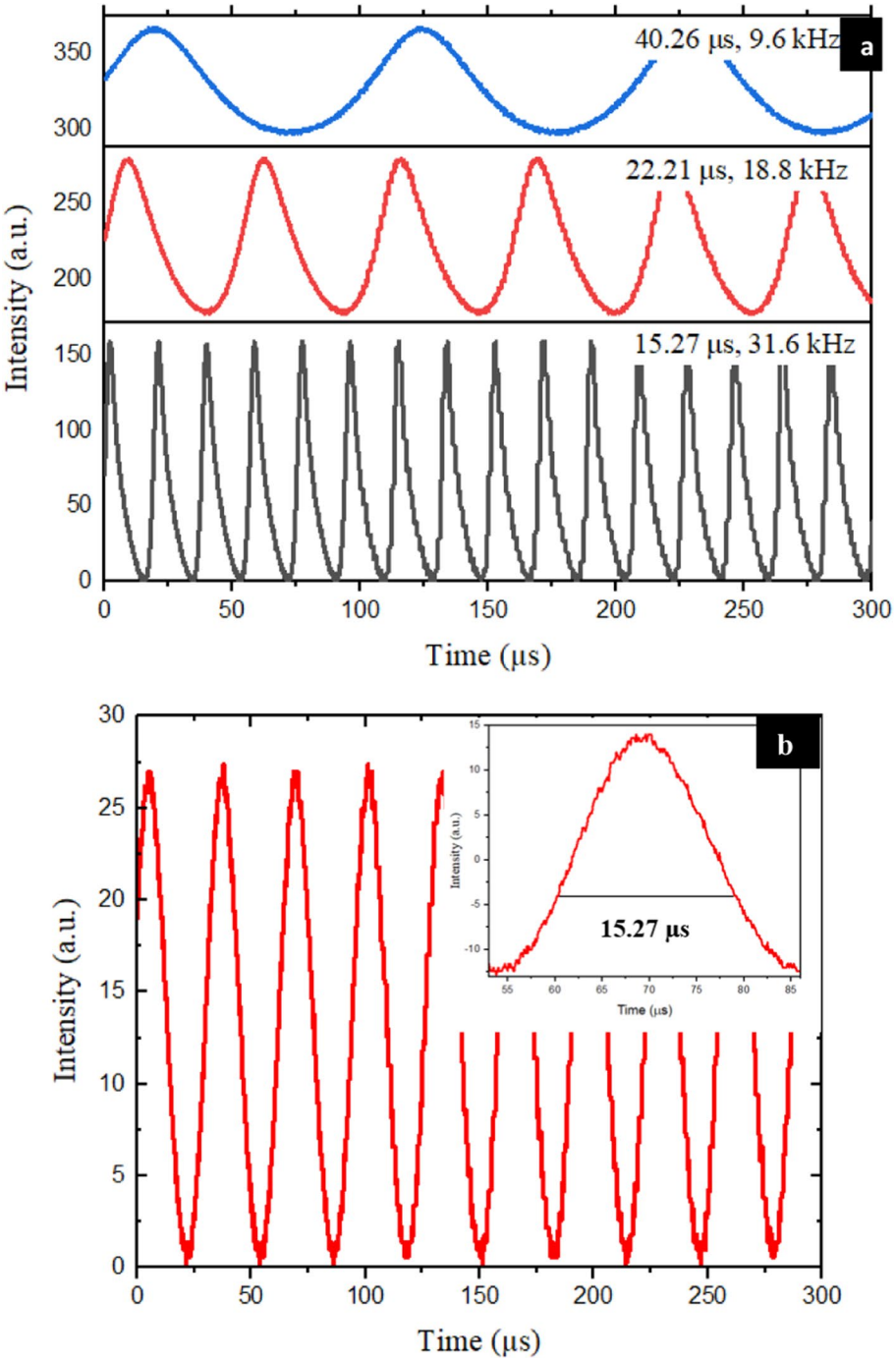

Fig. 12 Oscilloscope trace for erbium-doped fiber laser with boron carbide at **a** varying pump power, and **b** pump power of 275 mW, with inset of 3db pulse duration

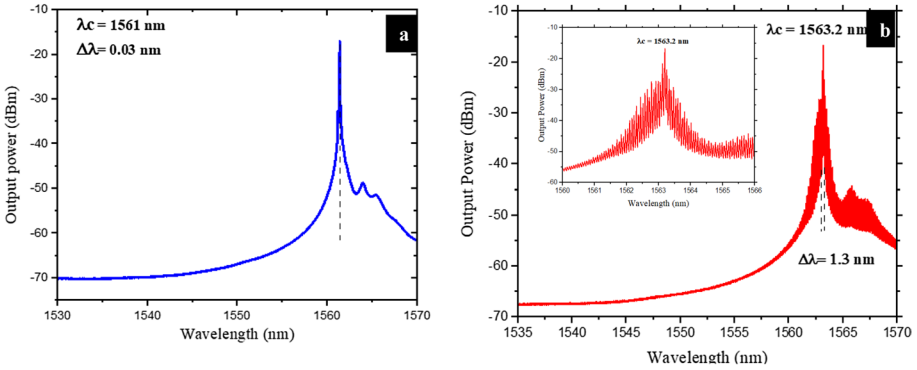

Fig. 13 Optical spectrum of EDFL. **a** Without SA, and **b** with B_4C-SA

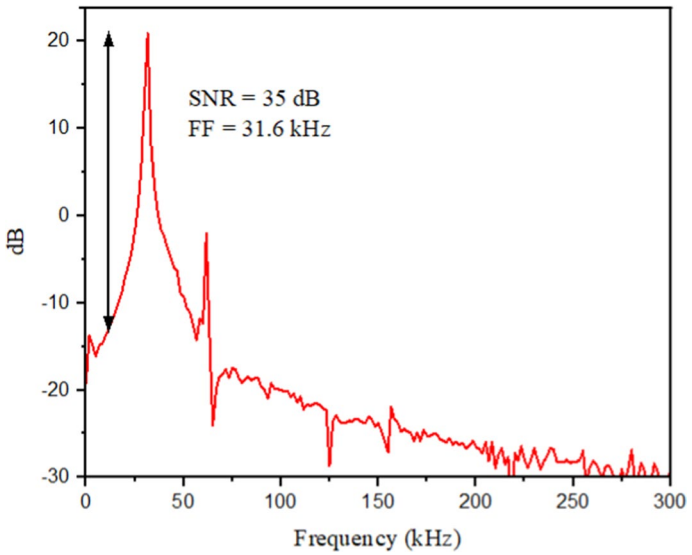

Fig. 14 The radio-frequency spectrum at an output power of 275 mW

Figure 12a displays the Q-switching pulse train of the EDFL at three different pump powers: 180 mW, 210 mW, and 275 mW. The pulses maintain consistent shape, frequency, and pulse duration. This figure reveals those variations in pump power result in changes to pulse characteristics such as repetition rate and pulse duration. Notably, decreasing the pump power from 275 to 180 mW leads to an observable increase in the duration of the pulse train. Figure 12b depicts the pulse train of the Q-switched fiber laser obtained through a digital oscilloscope trace, using a maximum pump power of 275 mW. The pulse train in Fig. 12b exhibits a pulse duration of 15.27 μs. At this pump power, the output power is approximately 171 μW, with a repetition rate of 31.6 kHz and a pulse energy of around 2.61 nJ. The large pulse duration may be due to the long laser cavity which leads

to the long cavity lifetime and this problem can be countered by reducing the length of the laser cavity and by improving the modulation depth of SA (Muhamad et al. 2019).

Figure 13a, b illustrates the spectral and temporal characteristics of the CW and Q-switched laser. The wavelengths of the laser output during continuous-wave and Q-switched operations, both without and with the SA, at a maximum pump power of 275 mW are displayed in Fig. 13(a, b). Incorporating the B_4C/PVA-SA into the laser cavity caused a shift in the peak laser wavelength from 1561 nm to 1563.2 nm. The Q-switched laser demonstrated a spectral bandwidth of 1.3 nm, which is wider than the 0.03 nm bandwidth of the CW laser.

Figure 14 exhibits the radio-frequency spectrum obtained when the laser operates at its maximum output power of 171 μW with a peak pump power of 275 mW. With this configuration, the pulse duration is 15.27 μs, and the repetition rate is 31.6 kHz, demonstrating that as the pumping power increases, the pulse frequency also rises, as depicted in Fig. 11a. The analysis of the amplitude of the first peak in Fig. 14 reveals a favorable signal-to-noise ratio, indicating a value of 35 dB. This confirms the relative stability of the generated pulses. The generation of Q-switching relies on the saturable absorption mechanism of nonlinear optical material, as discussed in previous research (Asghar et al. 2022).

Table 1 compares the passively Q-switched fiber laser used in this research to other comparable systems using various SAs. The output performance of the suggested laser system can be observed in the table to be equivalent, and in some cases even better, than that of prior reports, demonstrating the viability of B_4C as SA for Q-switched pulse production.

5 Conclusion

A Q-switched pulse laser using EDFL as the gain medium has been experimentally implemented with a new SA material, namely B_4C/PVA to operate at good stability. We used a B_4C suspension composited with PVA to construct a B_4C-doped PVA film as a fiber-compatible SA. When inserting the B_4C/PVA SA into an EDFL passively Q-switched laser, pulse duration, pulse repetition rate, and output power corresponded to 15.27 μs, 31.6 kHz, and 171 μW respectively. Based on experimental observations, we do confirm that B_4C-NPs exhibit nonlinear saturable absorption properties ($n_{2\ =}\ 5.591\times10^{-6}$ cm^2/W, $\beta = 0.011$ cm/W) and show appropriate potential to perform as Q-switches for pulsed fiber lasers.

Acknowledgements The authors are extremely grateful to the University of Technology- Iraq for its outstanding assistance.

Author contributions All authors co-implemented the experimental setup, co-analysed the data, co-wrote, and revised the main manuscript text. All authors contributed equally.

Funding The authors declare no Fund.

Availability of data, code, and materials Requests should be addressed to any author.

Declarations

Conflict of interest The authors declare no conflicts of interest.

Consent to participate Not applicable.

Table 1 Performance comparison of Q-switched over different SAs at 1.5 μm region

SA-material	Threshold Pump Power (mW)	Central Wavelength (nm)	Modulation depth (%)	Pulse duration (μs)	Pulse repetition rate (kHz)	References
Rhenium disulfide (ReS_2)	0.28	1557.3	0.12	5.496	19	Mao et al. (2017b)
Black phosphorus (BP)	10.4	1550	19.5	9.35	18	Jiang et al. (2015)
Graphene	57.2	1550		3.2	53.2	Zhang et al. (2012)
Telluride nanosheets	46	1563.7	0.97	5.196	47.61	Zhang et al. (2020)
Bismuth telluride (Bi_2Te_3)	67	1510.9 to 1589.1	22	13	12.82	Chen et al. (2013)
Boron Carbide (B_4C)	180	1563.2	2.3	15.27	31.6	This work

Consent for publication Not applicable.

References

Abdalhadi, A.H., et al.: Titania-carbon nanocomposite as a saturable absorber for generation passively ytterbium-mode locked pulses. Opt. Mater. **112**, 110728A (2021)

Ahmad, H., et al.: Cu 2 Te-PVA as saturable absorber for generating Q-switched erbium-doped fiber laser. Opt. Quant. Electron. **53**, 1–10 (2021)

Al-Hiti, A.S., et al.: Passively Q-switched 2 μm fiber laser with WO3 saturable absorber. Opt. Fiber Technol. **75**, 103193 (2023)

Alizadeh, M., Alizadeh, M., Amini, R.: Structural and mechanical properties of Al/B_4C composites fabricated by wet attrition milling and hot extrusion. J. Mater. Sci. Technol. **29**(8), 725–730 (2013)

Asghar, H., et al.: A novel technique for the fabrication of a saturable absorber for fiber lasers: pulsed laser deposition. Laser Phys. **19**, 075106 (2022)

Baharom, M., et al.: Lutetium oxide film as a passive saturable absorber for generating Q-switched fiber laser at 1570 nm wavelength. Opt. Fiber Technol. **50**, 82–86 (2019)

Bao, R.: Semiconducting Boron Carbide Thin Films: Structure, Processing, and Diode Applications. Rensselaer Polytechnic Institute, Troy (2010)

Bret, G., Gires, F.: Giant-pulse laser and light amplifier using variable transmission coefficient glasses as light switches. Appl. Phys. Lett. **4**(10), 175–176 (1964)

Caretti, I., et al.: Boron carbides formed by coevaporation of B and C atoms: Vapor reactivity, B × C 1–x composition, and bonding structure. Phys. Rev. B **77**(17), 174109 (2008)

Chang, B., et al.: Characterization of boron carbide nanoparticles prepared by a solid state thermal reaction. Appl. Phys. A **86**, 83–87 (2007)

Chen, Y., et al.: Large energy, wavelength widely tunable, topological insulator Q-switched erbium-doped fiber laser. IEEE J. Sel. Top. Quantum Electron. **20**(5), 315–322 (2013)

Chen, B., et al.: Q-switched fiber laser based on transition metal dichalcogenides MoS2, MoSe2, WS2, and WSe2. Opt. Express **23**(20), 26723–26737 (2015)

Du, X.-W., et al.: Face-centered-cubic Si nanocrystals prepared by microsecond pulsed laser ablation. J. Appl. Phys. **102**(1), 013518 (2007)

Fluck, R., et al.: Passively Q-switched 1.34-μm Nd: YVO4 microchip laser with semiconductor saturable-absorber mirrors. Opt. Lett. **22**(13), 991–993 (1997)

Guo, Z., et al.: From black phosphorus to phosphorene: basic solvent exfoliation, evolution of Raman scattering, and applications to ultrafast photonics. Adv. Funct. Mater. **25**(45), 6996–7002 (2015)

Guo, Y., et al.: Exfoliation of boron carbide into ultrathin nanosheets. Nanoscale **13**(3), 1652–1662 (2021)

Haryński, Ł, et al.: A facile method for Tauc exponent and corresponding electronic transitions determination in semiconductors directly from UV–Vis spectroscopy data. Opt. Mater. **127**, 112205 (2022)

Hassan, H., Munshid, M.A., Abdulhadi, A.-J.: L-band dual wavelength passively Q-switched erbium-doped fiber laser based on tellurium oxide nanoparticle saturable absorber. Laser Phys. **30**(2), 025101 (2019)

Hassan, H., et al.: Passive Q-switching using Lead Sulfide suspension as a saturable absorber in 1.5 μm region. Opt. Fiber Technol. **52**, 101969 (2019)

Hassan, H., Munshid, M.A., Abdulhadi, A.-J.: Tellurium-nanorod-based saturable absorber for an ultrafast passive mode-locked erbium-doped fiber laser. Appl. Opt. **59**(4), 1230–1236 (2020)

Ismail, E.I. et al.: Copper nanoparticles-chitosan based saturable absorber in passively Q-switched erbium-doped fiber laser. In: AIP Conference Proceedings. 2020. AIP Publishing LLC (2020)

Jasem, I.N., Abdullah, H.H., Jalal Abdulrazzaq, M.: Dual-wavelength passively Q-switched erbium-doped fiber laser incorporating calcium carbonate nanoparticles as saturable absorber. J. Nanotechnol. **2023**, 1–11 (2023)

Jeon, J., Lee, J., Lee, J.H.: Numerical study on the minimum modulation depth of a saturable absorber for stable fiber laser mode locking. JOSA B **32**(1), 31–37 (2015)

Jiang, T., et al.: Ultrafast fiber lasers mode-locked by two-dimensional materials: review and prospect. Photonics Res. **8**(1), 78–90 (2020)

Jiang, T., et al.: Black phosphorus as a new broadband saturable absorber for infrared passively Q-switched fiber lasers. arXiv preprint arXiv:1504.07341 (2015)

Kim, B., et al.: Tunable microsecond Q-switched fiber laser using an all-fiber deionized water saturable-absorber. J. Lumin. **258**, 119773 (2023)

Kumar, S.A., Senthilselvan, J., Vinitha, G.: Third order nonlinearity and optical limiting behaviors of Yb: YAG nanoparticles by Z-scan technique. Opt. Laser Technol. **109**, 561–568 (2019)
Liu, W., et al.: Ultrafast photonics of two dimensional AuTe2Se4/3 in fiber lasers. Commun. Phys. **3**(1), 15 (2020a)
Liu, W., et al.: SnSSe as a saturable absorber for an ultrafast laser with superior stability. Opt. Lett. **45**(2), 419–422 (2020b)
Liu, S., et al.: Application prospects of boron nitride as a novel saturable absorber device for ultrashort pulse generation in fiber lasers. J. Mater. Chem. C **9**(28), 9021–9027 (2021)
Luo, Z.-C., et al.: 2 GHz passively harmonic mode-locked fiber laser by a microfiber-based topological insulator saturable absorber. Opt. Lett. **38**(24), 5212–5215 (2013)
Luo, Z., et al.: 1.06 μm Q-switched ytterbium-doped fiber laser using few-layer topological insulator Bi2 Se3 as a saturable absorber. Opt. Express **21**(24), 29516–29522 (2013)
Mao, D., et al.: Nonlinear saturable absorption of liquid-exfoliated molybdenum/tungsten ditelluride nanosheets. Small **12**(11), 1489–1497 (2016)
Mao, D., et al.: Q-switched fiber laser based on saturable absorption of ferroferric-oxide nanoparticles. Photonics Res. **5**(1), 52–56 (2017a)
Mao, D., et al.: Passively Q-switched and mode-locked fiber laser based on an ReS2 saturable absorber. IEEE J. Sel. Top. Quantum Electron. **24**(3), 1–6 (2017b)
McClung, F.J., Hellwarth, R.W.: Giant optical pulsations from ruby. Appl. Opt. **1**(101), 103–105 (1962)
Mondal, S., Banthia, A.K.: Low-temperature synthetic route for boron carbide. J. Eur. Ceram. Soc. **25**(2–3), 287–291 (2005)
Muhamad, N.H., et al.: Bismuth (III) telluride-polyethylene oxide as passive saturable absorber. J. Phys. Conf. Ser. **1151**, 012002 (2019)
Muhammad, N., et al.: Q-switched fiber laser using a polysulfone membrane enhanced with biosynthesized zinc oxide and titanium dioxide nanoparticles for use as saturable absorber. Laser Phys. **32**(6), 065101 (2022)
Nersisyan, H.H., et al.: Polymer assisted approach to two-dimensional (2D) nanosheets of B_4C. Chem. Eng. J. **281**, 218–226 (2015)
Norizan, N.A.A., et al.: Q-switched erbium-doped fiber laser incorporating zinc oxide in polyvinyl alcohol as passive saturable absorber. J. Telecommun. Electron. Comput. Eng. **10**(2–7), 27–31 (2018)
Pierson, H.O.: Handbook of Refractory Carbides & Nitrides: Properties, Characteristics, Processing and Applications. William Andrew, Park Ridge (1996)
Sadeq, S.A., et al.: Copper oxide nanomaterial saturable absorber as a new passive Q-switcher in erbium-doped fiber laser ring cavity configuration. Results Phys. **10**, 264–269 (2018)
Saritha Devi, H., et al.: Optical emission diagnosis of boron carbide synthesized using natural carbon precursors. Opt. Spectrosc. **125**, 928–932 (2018)
Seifert, E., et al.: Investigations on retinal pigment epithelial damage at laser irradiation in the lower microsecond time regime. Invest. Ophthalmol. vis. Sci. **62**(3), 32–32 (2021)
Shakaty, A.A., et al.: Q-switched erbium-doped fiber laser based on nanodiamond saturable absorber. Opt. Laser Technol. **146**, 107569 (2022)
Siniaeva, M., et al.: Laser ablation of dental materials using a microsecond Nd: YAG laser. Laser Phys. **19**, 1056–1060 (2009)
Sobon, G., Sotor, J., Abramski, K.M.: Passive harmonic mode-locking in Er-doped fiber laser based on graphene saturable absorber with repetition rates scalable to 2.22 GHz. Appl. Phys. Lett. **100**(16), 161109 (2012)
Tao, X., et al.: B_4C-nanowires/carbon-microfiber hybrid structures and composites from cotton T-shirts. Adv. Mater. **22**(18), 2055–2059 (2010)
Thevenot, F.: Boron carbide—a comprehensive review. J. Eur. Ceram. Soc. **6**(4), 205–225 (1990)
Tu, J., et al.: Experimental characterization of a micro-hole drilling process with short micro-second pulses by a CW single-mode fiber laser. Opt. Lasers Eng. **55**, 275–283 (2014)
Wang, N., et al.: Passively Q-switched ytterbium-doped fiber laser with ReSe2 saturable absorber. Opt. Laser Technol. **116**, 300–304 (2019)
Wu, K., et al.: WS 2 as a saturable absorber for ultrafast photonic applications of mode-locked and Q-switched lasers. Opt. Express **23**(9), 11453–11461 (2015)
Wu, D., et al.: Saturable absorption of copper nanowires in visible regions for short-pulse generation. IEEE Photonics J. **8**(4), 1–7 (2016)
Xia, Y., et al.: One-dimensional nanostructures: synthesis, characterization, and applications. Adv. Mater. **15**(5), 353–389 (2003)
Yadav, R.K., Sharma, R., Omar, G.J., Aneesh, J., Adarsh, K.V.: Ultrafast Broadband Saturable Absorption inSb2Se3 Nanowires. Procedia Eng. **216**, 168–174 (2017)

Yang, S., et al.: Generation of Q-switched and mode-locked pulses based on PbS/CdS saturable absorbers in an Er-doped fiber laser. J. Mater. Chem. C **10**(15), 5956–5961 (2022)
Zhang, H., et al.: Graphene mode locked, wavelength-tunable, dissipative soliton fiber laser. Appl. Phys. Lett. **96**(11), 111112 (2010)
Zhang, L., et al.: Passively Q-switched fiber laser based on graphene saturable absorber. Laser Phys. **22**, 433–436 (2012)
Zhang, W., et al.: Passively Q-switched and mode-locked erbium-doped fiber lasers based on tellurene nanosheets as saturable absorber. Opt. Express **28**(10), 14729–14739 (2020)